Design, manufacturing and characterization of aero-elastically scaled wind turbine blades for testing active and passive load alleviation techniques within a ABL wind tunnel

2014 J. Phys.: Conf. Ser. 524 012061

(http://iopscience.iop.org/1742-6596/524/1/012061)

Design, manufacturing and characterization of aero-elastically scaled wind turbine blades for testing active and passive load alleviation techniques within a ABL wind tunnel.

Filippo Campagnolo[1,2], Carlo L Bottasso[1,2] and Paolo Bettini [2]

[1] Lehrstuhl für Windenergie, Technische Universität München, Boltzmannstraße 15, Garching bei München, Germany

[2] Dipartimento di Scienze e Tecnologie Aerospaziali, Politecnico di Milano, Via La Masa 34, Milano, Italy

E-mail: filippo.campagnolo@tum.de, carlo.bottasso@tum.de, paolo.bettini@polimi.it

Abstract. In the research described in this paper, a scaled wind turbine model featuring individual pitch control (IPC) capabilities, and equipped with aero-elastically scaled blades featuring passive load reduction capabilities (bend-twist coupling, BTC), was constructed to investigate, by means of wind tunnel testing, the load alleviation potential of BTC and its synergy with active load reduction techniques. The paper mainly focus on the design of the aero-elastic blades and their dynamic and static structural characterization. The experimental results highlight that manufactured blades show desired bend-twist coupling behavior and are a first milestone toward their testing in the wind tunnel.

1. Introduction and motivation

Load reduction techniques for wind turbines can be broadly categorized into two families: active and passive. Within the active category, IPC [1] has the potential of reducing fatigue and possibly ultimate loads, but at the cost of increased duty cycle (ADC [1]). Passive load reduction techniques are instead based on the idea of designing a structure that, when loaded, deforms so as to induce a load reduction. One classical solution to achieve this structural behavior is to design blades with some degree of bend-twist coupling (BTC), and the literature [2] clearly shows the potential benefits of BTC.

Recently, it has been also shown in Ref. [3] that, by properly designing coupled BTC blade, one can achieve not only significant load alleviation on the wind turbine sub-structures, but also the pitch actuator duty cycle (ADC) is much reduced. This result is of potential interest, because it opens the way to a synergistic combination of passive and active load control technologies given that BTC and IPC can both mitigate loads, but BTC reduces ADC while IPC increases it. Therefore, it appears possible to have a combined load reduction effect, larger than one would get by adopting one single technology, while limiting the effects on ADC.

The majority of the research concerning the aero-elasticity of rotating blades with BTC focuses on simulations, while experiments [4] mainly focused on the investigation of the sole static/dynamic properties of full size wind turbine blade. Nevertheless, on the basis of authors'

knowledge, no experiments focused on the study of the aero-elasticity of BTC blades, as well as on the potential synergy between active control laws and passive control techniques, have been conducted in the past: we therefore think there is the need of further experimental activities. Faced with this need, the preferred solution would be field-testing; however, these usually present some hurdles: complexity to have full and accurate knowledge of the environmental testing conditions, relevant testing costs and times. As an alternative to field testing, one can resort to the use of scaled models which means, when wind energy applications are involved to, testing in the wind tunnel. In this regard, it is authors' opinion that wind tunnel activities could support investigations also in the field of aero-servo-elasticity, as highlighted in Ref. [5].

In the research described in this paper, a scaled wind turbine model featuring individual pitch control capabilities and equipped with aero-elastically scaled blades with BTC was constructed to investigate, by means of wind tunnel testing, the load alleviation potential of the concept and its synergy with active load reduction techniques. This paper mainly focus on the design of the aero-elastic blades, their manufacturing and static/dynamic structural characterization and it is a first milestone toward the testing of the wind turbine model here presented in an atmospheric boundary layer wind tunnel.

2. Scaled wind turbine model

The wind tunnel used for testing the model will be the **GVPM** of the Politecnico di Milano, which features a 4m $\times$ 3.84 m test chamber, mainly used for aeronautical-related applications, and a boundary layer 13.84 m $\times$ 3.84 m by 36 m test chamber, which permits to perform tests on relatively large models with low blockage effects and is primarily used for civil and wind engineering applications.

The model geometry, loosely based on the Innwind 10 MW Reference Wind Turbine, has been conceived to allow its testing within the wind tunnel of the Politecnico di Milano. The diameter of the model rotor, equal to $\approx$1.9 m (geometric scaling factor $n_l \approx 1/93$), has been fixed with the aims of avoiding excessive blockage effects. Once fixed the diameter, we proceed as reported in Ref. [5] for the formulation of the scaling laws. The model rotor speed, equal to $\approx$365 rpm (time scaling factor $n_t \approx 1/38$), has been selected seeking for the best compromise between limiting the unavoidable Reynolds mismatch due to scaling and the need to limit the scaled-up of the time, in order to avoid excessive control bandwidth.

Once defined the length and time scaling ratios, the scaling factors of the principal physical quantities were easily derived and table (1) reports the main ones.

Table 1. Scaling factors used for mapping the Innwind Reference Wind Turbine into the model characteristics.

Quantity	Scaling factor	
Length	n_l	$1:93.25$
Rotor Speed	n_Ω	$38:1$
Wind Speed	$n_l n_\Omega$	$1:2.45$
Bending Stiffness	$n_l^6 n_\Omega^2$	$1:4.55\cdot 10^8$
Mass Distribution	n_l^2	$1:8695$
Reynolds	$n_l^2 n_\Omega$	$1:225$

The aerodynamic shape of the model rotor blades was conceived to achieve a realistic energy conversion process, i.e. same tip speed ratio as well as realistic aerodynamic thrust and power. For this purpose, the blade was designed using airfoils developed for Reynolds around 50000-60000 and equipped with transition strip. The AH79-100C and WM006 profiles were used (Fig. 1), given

that their proficiency at low Reynolds had already been proven [5]. The former airfoil extends for $\frac{r}{R} = \eta \in [0.146, 0.451]$ and the latter for $\eta \in [0.697, 1]$. In the blade inner region, the inboard airfoil smoothly deforms into the blade root cylinder, which extends for $\eta \in [0.0, 0.021]$.

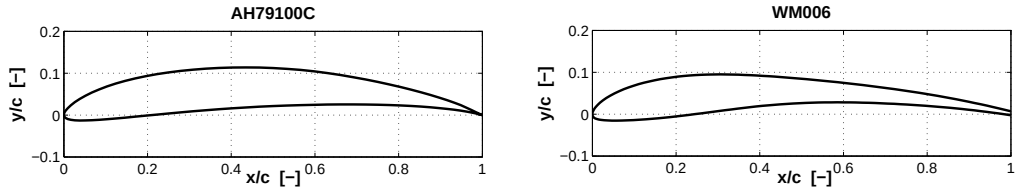

Figure 1. Model airfoils shape.

The span-wise chord distribution of the model blade was quite similar to the one of the Innwind reference machine, but with the following minor modifications:

- the chord distribution (Fig. 2(a)) has been slightly increased in the inboard part of the blade and at the tip, so as to make the model airfoils operate at Re higher than 50000 in a wider part of the blade (Fig. 2(b));
- the blade chord has been slightly decreased in the central part of the blade so as to have almost the same scaled model and full scale rotor solidity.

To account for the change of airfoils between the full scale and scaled blades, as well as for the different chord distribution, the blade twist was modified to yield an optimal span-wise distribution of the axial induction factor (Fig. 2(c)).

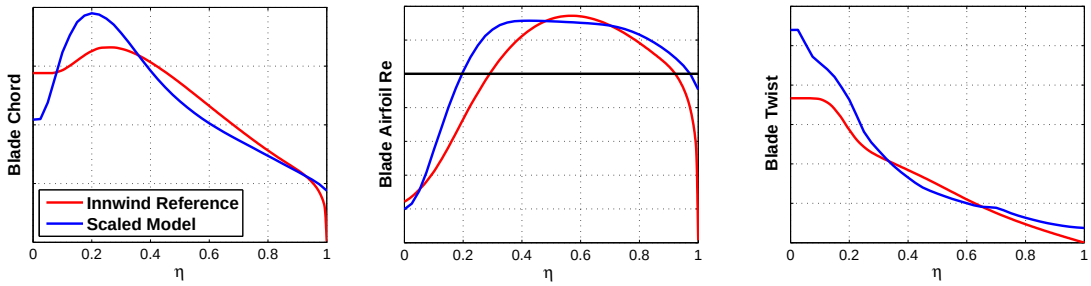

(a) Blade chord (b) Blade Re at rated power (c) Blade twist

Figure 2. Comparison between the scaled reference and the model span-wise distribution of the blade chord (a), airfoil Reynolds number at rated power (b) and blade twist(c).

The model have been realized flexible and capable of representing the mutual interactions of aerodynamic, elastic and inertial forces. A comprehensive onboard sensorization of the machine allows to accurately measure the aerodynamic torque, the bending loads on the shaft, the rotor azimuth and accelerations at tower top. The aero-elastic blades are also highly sensorized. Strain gauge bridges are installed at the blade root providing measures of the bending moments, while optical fibers equipped with FBG (Fibre Bragg Grating) sensors are embedded in the blade and allow the reconstruction of the loads approximately at one third of the blade span. Fibers are coupled together and connected with the external optical sensing interrogator by using a FORJ (Fiber Optic Rotary Joint) integrated in an electro–optical slip ring.

In the model, as well as in the full-scale wind turbine, the control action is performed by varying the blades pitch and the generator torque. For each blade, the pitch actuation is demanded to

a small brushed motor, while the torque actuation is provided by a brush-less motor driven by a 4-quadrant control board. The electrical onboard sensors signals are sampled by the analog acquisition modules of an industrial `Bachmann M1` hard-real-time system. Collective pitch and torque PI controller, as well as higher harmonic IPC controllers, are compiled to the `M1 CPU`. The control outputs are sent to the actuators control boards via the `M1 CAN` module or by analog output. Further details about the controllers implementation can be found in Ref. [5] and reference therein.

3. Aero-elastic blades: manufacturing technology and design tool

The design and production of the aero-elastic blades was a complex challenge, given that the following requirements should be accomplished:

- external shape consistent with the designed one, with good surface finishing;
- realistic distribution of the inertial and stiffness properties with respect to the ones specified by the scaling factors (see table (1), which implies also requirements on the placement of the blade natural frequencies.
- controllable and reproducible manufacturing process, so as to produce a set of identical blades.

Among the design complications were the extremely complex blade shape: it transforms from the cylindrical root to airfoils whose thickness is about $0.10c$, with variable chord c, thickness and twist. Furthermore, the target mass was equal to slightly over than 50 [g], while the first flap-wise frequency had to be greater than the 3-per-rev.

3.1. Blade layout

The blade layout shown in Fig. (3) was inspired by what already done by other wind tunnel experimenters [6, 7]. The bending stiffness is mainly provided by two properly sized and located composite spars made of unidirectional carbon fibers; this solution allows to ensure the proper distribution of the flap-wise stiffness using a moderate fraction of the blade target mass, to provide bend-twist coupling by rotating the fiber in the spar and to embed the optical fiber sensors between the spar carbon plies.

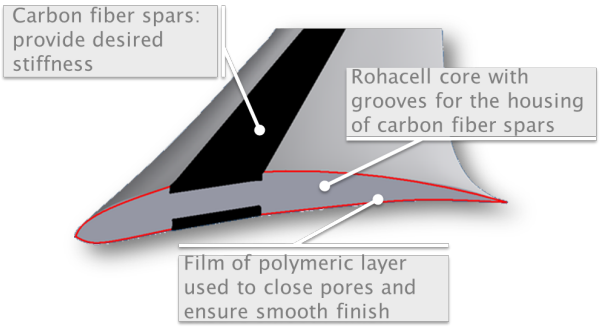

Figure 3. Aero-elastic model blade layout.

A `Rohacell` core is used to avoid any deformation of the blade sections shape due to aerodynamic pressure, as well as to bind the carbon spars together and increase buckling stability. All this is achieved using a small and predictable fraction of the blade target mass, with little increase of the cross-sectional stiffness; furthermore, the `Rohacell` exhibits good deformability properties if subjected to conveniently high level of pressure, like that developed by the mold action (see §3.2), and resists at high cure temperature. An uncured polymeric layer is used to

cover the blade surface and to provide good and smooth finishing by filling the Rohacell pore. Moreover, it contributes to increase the torsional stiffness with moderate effect on the bending stiffness. Finally a machined steel component is embedded in the root before starting the cure process, allowing the subsequent assembly of the blade on the hub. s. Finally a machined steel component is embedded in the root before starting the cure process, allowing the subsequent assembly of the blade on the hub.

3.2. Blade manufacturing

The entire manufacturing process has been set up with the goal of manufacturing good quality blades conform with the design requirements and with a high level of reproducibility. The Rohacell cores are produced by CNC machining so as to have their shape close to the blade one. However, the cores are manufactured with a thickness distribution slightly greater than the blade one, so as to force the core occupy a minor volume once closed the mold used to apply and shape the external polymeric layer. With this stratagem the core exerts, as a reaction, an adequate pressure level on the inner of the mold in agreement with the curing process of the epoxy resin. The core is also conveniently machined in order to create, over its external surface, the grooves which house the carbon spars and guide their placement during the assembly.

The spars curing process is carried out prior to assembly the entire blade. Due to their complex shape carbon pre-preg plies are cut using an automatic cutting tool and then stacked in accordance to the ply-book. The optical fibers are embedded between the two outer plies during the lamination process and FBG sensors are placed at the desired location. A dedicated mold is specifically conceived and produced for letting the optical fibers get out the spars without causing damage.

In this way, it is possible to manufacture highly accurate and reproducible carbon reinforcements strictly in accordance to the design output. More details about the blade components manufacturing are reported in Ref. [8].

Once the blade sub-components are produced, it is possible to proceed with the final assembly and, immediately after, the final curing process. For this purpose, an alloy female mold is used, while the assembly is characterized by the phases shown in Fig. (4) and listed below:

- a thin film of glue is used for sticking together the Rohacell core and the metal root part;
- the two spars are laid down on the Rohacell core surfaces and a thin layer of glue is used to ensure the bonding between the parts;
- a layer of glue is laid up over the core using the mold as support base, so as to avoid breaking the fragile core; the resin film is laid on one side of the blade, wrapped around the leading edge and then laid on the other side, so as to form a continuous and homogeneous coating;
- finally, such an artifact is placed between the two mold halves and the closure is performed using several uniformly spaced screws, so as to generate uniform and high enough pressure. The metal root part is then fixed at the mold support blocks, where small holes allow the way out of the optical fibers without causing damage.

Once finished the assembly procedure, the curing process takes place in the oven with monitored temperature. At the end of the production process modest finishes are necessary to obtain a high-quality aero-elastic blade.

3.3. Blade design tool

The structural design of the model aero-elastic blade was a complex and challenging task, since the design had to account for the definition of the structural layout, the choice of the materials and the sizing of the structural members. Given layout and materials, the sizing problem had to be performed so as to have the structural properties of the scaled model blade close to the

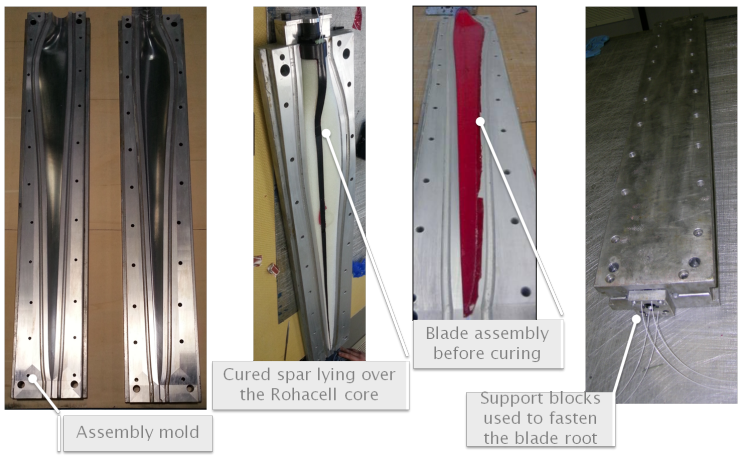

Figure 4. Pictures and description of the blade sub-components assembly.

scaled one of the reference blade. Moreover, the correct aero-elastic scaling of the model required the matching of the lowest 3 non-dimensional frequencies of the system, i.e. two flap and one lag bending modes.

The main challenge of this design problem came from the need to have a fast design tool that accounts for all the requirements listed above and, at the same time, to capture the local effects in complex 3D structures made with anisotropic composite materials, as the model blade is. The multi-level design procedure here used, and briefly described below, is based on the works published in Refs. [9, 10]. As a starting point for the optimization, an initial definition of the blade structural configuration and associated material properties is required. Next, the primary design variables are defined at selected span-wise sections while intermediate values along the blade span are interpolated using shape functions. Equivalent cross sectional stiffness and inertial data are then generated using the approach of Ref. [11]. The obtained sectional beam data are used to develop a beam-like multibody model of the blade. The automatic computation of the model beam eigenvalues is then performed, whereby constraint conditions ensuring the right placement of the model natural frequencies are included in the optimization process. Furthermore, additional constraints on the unknown design parameters are included, while the cost function of the optimization problem is a measure of the difference between the model and full-scale span-wise distributions of the blade edge-wise stiffness. We decided to use this cost function since the model blade airfoils are much thinner than those used in the target blade, which implies that the achievable ratio edgewise-flapwise stiffness will be greater than target blade one. With this cost function the solution which minimizes this unavoidable discrepancy is sought.

Successively, a 3D CAD model of the optimal blade geometry, precisely accounting for all components of the blade (spar caps, external skin, `Rohacell` core and blade root insert), is automatically generated as described in Ref. [9], while the meshing is performed with the commercial software `HyperMesh`. The 3D FEM model provides the framework for a fine-level verification of the design constraints, as the detailed model reveals effects that may have been overlooked by the coarse quasi-3D model composed of 1D spatial beam and 2D cross sectional models as, for example, local effects at regions with rapidly changing geometry in the span-wise direction. In case constraint violations are detected at the fine-level, the coarse optimization loop is repeated with constraint bounds that are tightened proportionally to the violation amount; coarse and fine level iterations are repeated until an optimal design that satisfies the constraint conditions at the finest description level is obtained.

4. Applications and results

In the following sections the design, manufacturing and testing of the aero-elastic blade featuring BTC is presented.

4.1. Materials selection

For this project, the `HM M50J 100 EU334 32.5%` uni-directional high-modulus pre-preg was selected for the production of the carbon spars on the basis of its very high module to density ratio. With regard to the filler, the `Rohacell WF71` was chosen, given it was a good compromise between low density and not excessive cells size. For the external skin a film of `Scotch Weld®AF 163-2K` was used; this epoxy structural adhesive has a curing temperature equal to that of the UD carbon and its supporting carrier provides good drapability, fundamental given the complex and doubly curved blade surface. Considering that the design of the blade is highly sensitive to the materials properties, a complete characterization of the three materials used in the blade manufacturing was necessary. More details related to the materials characterization and properties are reported in Ref. [8].

4.2. Aero-elastic blades design

Before starting with the design process we tried to figure out how to generate sufficient bend-twist coupling with the adopted blade layout. For this purpose, the best approach resulted in introducing BTC to twist the blade sections so as to decrease the angle of attack, the so called twist-to-feather concept. Fully coupled design, where fibers are rotated in the spar of an angle equal to θ_{spar} and for the whole span-wise extension of the blade, was considered. A preliminary analysis highlighted that rotating the carbon fibers with an angle equal to θ_{spar}=3 deg generated a coupling, expressed as the coefficient $\alpha_s = K_{bt}/\sqrt{K_{fb}K_t}$ (with K_{fb}, K_t and K_{bt} respectively the local flap-wise bending, torsional and coupled bend-twist stiffness), similar to the ones reported in Ref. [3].

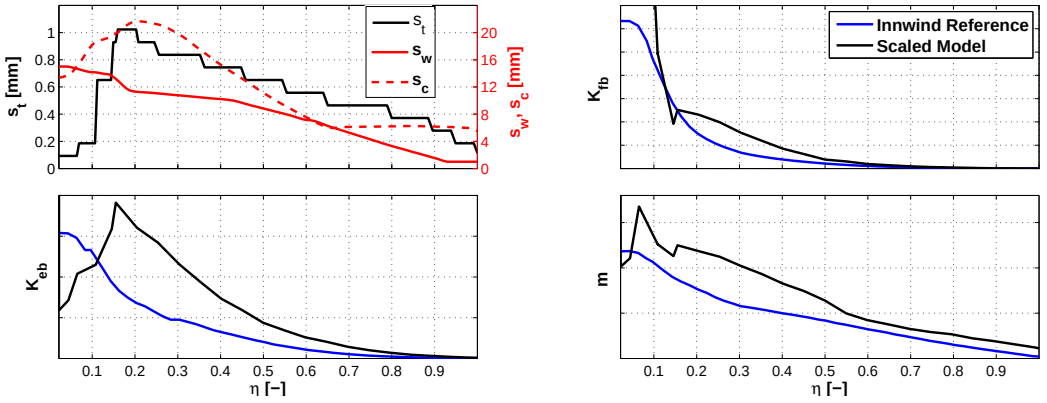

Figure 5. Comparison between the cross-sectional properties of the scaled model and target blades: flap-wise stiffness K_{flap} (up-right), edge-wise stiffness K_{edge} (down-left) and mass m (down-right), together with the span-wise distribution of the spars thickness, width and chord-wise location (up-left).

The design tool described in §3.3 was used to determine optimal distribution of the chord-wise location $s_c(\eta)$, width $s_w(\eta)$ and thickness $s_t(\eta)$ of the spars, which are plotted in Fig. (5). The model cross sectional flap-wise stiffness distribution matches well, once scaled-back, the one of the reference blade, while the mass distribution is moderately higher. In the outboard region of the

blade, the edge-wise stiffness distribution is instead higher with respect the reference one, given that the model airfoils are much thinner than those used in the Innwind machine. It is possible to note that this effect has been compensated by structurally weakening the blade in the inboard region, so as to satisfy the constraint on the 1^{st} edge-wise frequency placement.

Despite an over-weight of approximately 40% – in turn mainly due to the filler and glue weights and therefore not strongly affected by the design – the three first natural frequencies resulted being quite close to their targets. Moreover, Fig. (6) shows the comparison between the span-wise distribution of the coupling coefficient α of the model blade and of the optimal blade Sk+20&SC+05 of Ref. [3]. It is therefore possible to reasonably conclude that the designed blade is a realistic aero-elastic model of a 10 MW wind turbine blade providing also realistic bend-twist coupling capabilities.

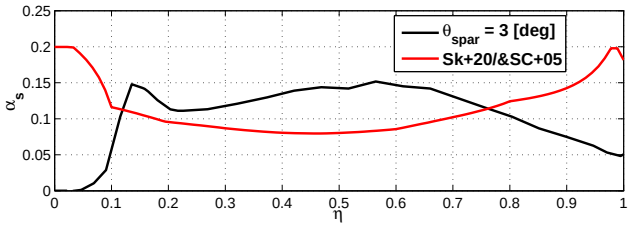

Figure 6. Coupling coefficient α of the model blade with θ_{spar}=3 deg, compared with the one of the optimal blade Sk+20&SC+05 of Ref. [3]

.

4.3. Manufacturing and structural characterization

The carbon-made plies with fibers rotated of 3 [deg] were produced starting from the mathematics of the plies flat pattern and using an automatic cutting tool, while four fiber optics with embedded FBG sensors were inserted between the two outer carbon plies during the lamination phase of the spars. The mass of the three manufactured blades, as well as their center of gravity span-wise position, were measured and found to be quite close to the design values, with errors in the range of 1-3%. Modal analysis was also carried out to characterize the dynamic properties of one of the three manufactured blades. The blade root was fixed to a steel-made plate that, in turn, was fixed to the laboratory floor, thus ensuring a perfectly rigid constraint. Impact hammer tests were performed using one miniaturized and lightweight (0.5 [g]) uni-axial PCB 352C22 accelerometer, while the structure was excited at 22 different locations (see Fig. 7) using an hammer instrumented with a load cell PCB 086B03, so as to being able to reconstruct, with a good accuracy, the eigen-shape associated to flap-wise and torsional modes.

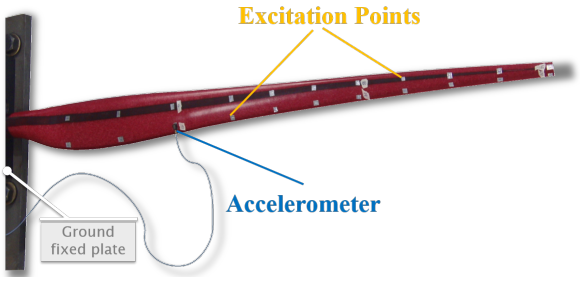

Figure 7. Hammer modal testing.

Eight flap-wise and torsional natural frequencies $\check{\omega}$, and related damping $\check{\zeta}$ and eigen-vectors $\check{\mathbf{\Phi}}$, have been identified on the basis of the measured FRFs, as well as two edge-wise modes were observed. Table (2) reports the comparison between the experimental $\check{(\cdot)}$ and numerical $\hat{(\cdot)}$ natural frequencies, as well as the value of the MAC$(\hat{\mathbf{\Phi}}_i, \check{\mathbf{\Phi}}_i)$ operator.

The comparison is quite satisfactory and specially the measured eigen-shape of the flap-wise modes well matches the corresponding numerical ones. Also the numerical values of the natural pulsations of the torsional and edge-wise modes well match the measured ones, while the 3D FE model overestimates the natural frequencies of the first flap-wise modes approximately 13%. This, however, will not imply higher loads then expected being the ratio $\frac{\check{\omega}_{1\,\mathrm{flap}}}{3\Omega_r}$, with $\check{\omega}_{1\,\mathrm{flap}}$ and $3\Omega_r$ respectively the 1^{st} flap-wise and three-per-rev pulsations, approximately equal 1.135, which means that resonant conditions in the operating envelope of the model are avoided.

Table 2. Measured natural frequencies compared with the ones computed on the 3D FE model.

Mode	$\check{\omega}$ [Hz]	$\check{\zeta}$ [%]	$\hat{\omega}$ $[Hz]$	$\frac{\check{\omega}-\hat{\omega}}{\check{\omega}}$ [%]	MAC
1^{st} Flap-wise	20.7	0.86	23.3	-12.7	0.99
1^{st} Edge-wise	33.73	-	35.7	-5.8	-
2^{nd} Flap-wise	55.1	0.74	62.2	-12.9	0.978
2^{nd} Edge-wise	109.69	-	112.5	-2.5	-
3^{rd} Flap-wise	115.9	0.85	132.5	-14.3	0.917
1^{st} Torsional	155.5	1.52	162.1	-4.2	0.563
4^{th} Flap-wise	194.2	1.25	227.5	-17.1	0.969
2^{nd} Torsional	240.6	1.51	254.4	-5.7	0.539
5^{th} Flap-wise	286.8	1.35	335.5	-16.9	0.824
3^{rd} Torsional	366.2	1.45	389.3	-6.3	0.463

Static tests were also performed with the blade fixed at its root and equipped with four saddles placed at $\eta = [0.206, 0.494, 0.796, 0.947]$. Dead loads were applied at each saddle in the vertical direction at three points **A**, **B** and **C** (see Fig. 8), with **B** aligned with the pitch axis. Three laser LAS8010 displacement transducers were used for each saddle to measure its vertical, horizontal and torsional deformations. The blade was subjected to various loads inducing either mostly flap-torsional or mostly edge-wise deformations. For the pure flap-wise tests saddles were loaded at central point. Similarly, for the flap-torsional tests, saddles were loaded at both lateral points, thus allowing to separate the deformation due to the torsional flexibility from that due to bend-twist coupling.

Fig. 9 shows the measured vertical $\check{\delta}_s$ and torsional $\check{\delta}_r$ displacements related to the load case with dead loads applied at point A. The comparison with the numerical $\hat{(\cdot)}$ displacements of the beam-like multibody model is quite satisfactory. Moreover, this load condition highlights the bend-twist coupling effect: the increment of the angle of attack (i.e. $\delta_r > 0$) due to torsion is indeed compensated by the deformation due to BTC, specially in the central area of the blade ($\eta \in [0.2, 0.8]$).

5. Conclusions and future activities

A scaled wind turbine model featuring IPC capabilities and equipped with aero-elastically scaled blades featuring BTC has been here presented. The proposed manufacturing technology, as well as the tool used for the blade design, have proven to be suitable for the production of a set of three identical aero-elastic blades featuring bend-twist coupling. The experimental tests showed that blades structural properties are realistic when compared to those of a multi-MW

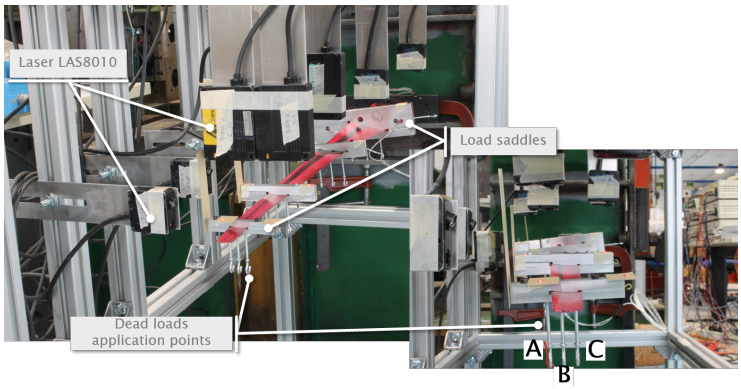

Figure 8. Static testing with dead loads.

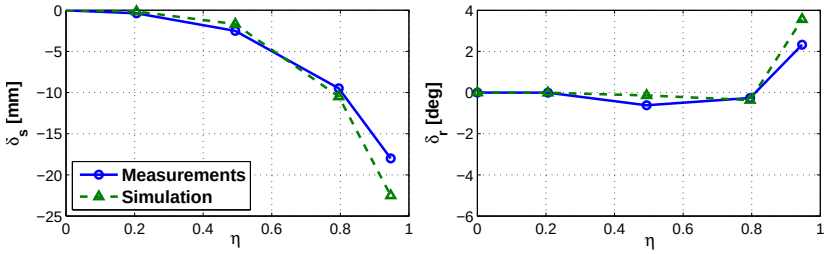

Figure 9. Comparison between experimental and numerical displacements.

wind turbine blade. Wind tunnel testing will be shortly conducted within the ABL test chamber of the Politecnico di Milano wind tunnel, and will concern the synergistic effect of active and passive loads reduction techniques.

Acknowledgements
The present project is funded within the EU FP7 framework program through Innwind. The authors wish to thank S. Cacciola and Prof. G. Sala of the Politecnico di Milano for numerous technical contributions in the development and testing of the experimental equipment.

References
[1] Burton T, Sharpe D, Jankings N and Bossanyi E 2001 *Wind Energy Handbook* (John Wiley & Sons)
[2] Cappellaro M and Kühn M 2010 Boundaries of bend twist coupling *TORQUE 2010, The Science of Making Torque from Wind*
[3] Bottasso C, Campagnolo F, Croce A and Tibaldi C 2013 *Wind Energy* **16** 1149–66
[4] Berring P, Branner K, Berggreen C and Knudsen H W 2007 Torsional performance of wind turbine Blades-Part I: Experimental investigation *16-th International Conference on composite materials*
[5] Bottasso C, Campagnolo F and Petrović V 2014 *Journal of Wind Engineering and Industrial Aerodynamics* **127** 11–28
[6] Hulskamp A W, van Wingerden J W, Barlas T, Champliaud H, van Kuik G, Bersee H E N and Verhaegen M 2011 *Wind Energy* **14** 339–354
[7] Jinsong B, Nagaraj V, Chopra I and Bernhard A 2008 *Journal of the american helicopter society* **53** 215–225
[8] Campagnolo F 2012 Wind tunnel testing of scaled wind turbine models: aerodynamics and beyond. *PhD thesis, Dipartimento di Ingegneria Aerospaziale, Politecnico di Milano.*
[9] Bottasso C, Campagnolo F and Croce A 2012 *Multibody System Dynamics* **27 (1)** 21–53
[10] Bottasso C, Campagnolo F, Croce A, Dilli S, Gualdoni F and Nielsen M 2013 *Multibody System Dynamics, publisched on-line*
[11] Giavotto V, Borri M, Mantegazza P and Ghiringhelli G 1983 *Computers & Structures* **16** 403–413